THE JOURNAL OF BIOLOGICAL CHEMISTRY VOL. 289, NO. 23, pp. 16565–16575, June 6, 2014

Functional Role for Piezo1 in Stretch-evoked Ca^{2+} Influx and ATP Release in Urothelial Cell Cultures*

Received for publication, November 9, 2013, and in revised form, April 11, 2014 Published, JBC Papers in Press, April 23, 2014, DOI 10.1074/jbc.M113.528638

Tatsuya Miyamoto[‡], Tsutomu Mochizuki[‡1], Hiroshi Nakagomi[‡], Satoru Kira[‡], Masaki Watanabe[§], Yasunori Takayama[§], Yoshiro Suzuki[§¶], Schuichi Koizumi[‖], Masayuki Takeda[‡], and Makoto Tominaga[§¶2]

From the [‡]Department of Urology, Interdisciplinary Graduate School of Medicine and Engineering, University of Yamanashi, 1110 Shimokato, Chuo, Yamanashi 409-3898, the [§]Division of Cell Signaling, Okazaki Institute for Integrative Bioscience (National Institute for Physiological Sciences), National Institutes of Natural Sciences, Higashiyama 5-1, Myodaiji, Okazaki, Aichi 444-8787, the [¶]Department of Physiological Sciences, Graduate University for Advanced Studies, Okazaki 444-8585, and the [‖]Department of Neuropharmacology, Interdisciplinary Graduate School of Medicine and Engineering, University of Yamanashi, 1110 Shimokato, Chuo, Yamanashi 409-3898, Japan

Background: The Piezo1 channel was recently identified as a genuine mechanosensor in mammalian cells.
Results: Urothelial cells exhibited a Piezo1-dependent increase in cytosolic Ca^{2+} concentrations in response to mechanical stretch stimuli, leading to ATP release.
Conclusion: Piezo1 senses extension of the bladder urothelium, which is converted into an ATP signal.
Significance: Inhibition of Piezo1 might provide a new treatment for bladder dysfunction.

The urothelium is a sensory structure that contributes to mechanosensation in the urinary bladder. Here, we provide evidence for a critical role for the Piezo1 channel, a newly identified mechanosensory molecule, in the mouse bladder urothelium. We performed a systematic analysis of the molecular and functional expression of Piezo1 channels in the urothelium. Immunofluorescence examination demonstrated abundant expression of Piezo1 in the mouse and human urothelium. Urothelial cells isolated from mice exhibited a Piezo1-dependent increase in cytosolic Ca^{2+} concentrations in response to mechanical stretch stimuli, leading to potent ATP release; this response was suppressed in Piezo1-knockdown cells. In addition, Piezo1 and TRPV4 distinguished different intensities of mechanical stimulus. Moreover, GsMTx4, an inhibitor of stretch-activated channels, attenuated the Ca^{2+} influx into urothelial cells and decreased ATP release from them upon stretch stimulation. These results suggest that Piezo1 senses extension of the bladder urothelium, leading to production of an ATP signal. Thus, inhibition of Piezo1 might provide a promising means of treating bladder dysfunction.

Bladder urothelium has classically been considered a passive barrier against water, ions, solutes, and infections. However, it is currently thought that urothelial cells are involved in sensory mechanisms in response to physical and chemical stimuli (1–4) and that bladder urothelium can sense bladder extension and respond to stimuli by releasing neurotransmitters, including ATP (5, 6). ATP released from the urothelium has an important role in acting on P2X receptors in afferent nerves to transmit signals of bladder filling (7). In this mechanosensory transduction system, the opening of stretch-activated channels (SACs)[3] is the first step, leading to various intracellular events. Most SACs are nonselective cation channels with high Ca^{2+} permeability (8), indicating that SACs convert mechanical force into Ca^{2+} influx. We hypothesized that SACs sense the extension of the bladder urothelium. The molecular candidates for SACs in mammals include two-pore domain K^+ channels, acid-sensing ion channels (ASICs), and the transient receptor potential (TRP) family of channels (4, 9–16).

Gating of the two-pore domain K^+ channels (TREK1, TREK2, and TRAAK) is regulated by mechanical perturbation of the cell membrane as well as polyunsaturated fatty acids, other lipids, and temperature (17–19). ASICs were initially implicated in mechanotransduction because they are essential for perception of touch (20, 21). On the other hand, TRPs sense thermal stimulation, and TRPV4 is involved in mechanosensation (22–25). In the mouse bladder urothelium, urothelial cells sense mechanical stretch stimuli via TRPV4 channels, which induce Ca^{2+} influx and contribute to ATP release upon extension (26). Although TRPs and ASICs are candidate mechanosensors of stretch stimulation, there is little unambiguous evidence indicating that these channels are directly mechanically gated. Moreover, these proteins do not fulfill all of the criteria for SACs. In other words, when expressed heterologously, none of these channels recapitulates the electrical signature of sensory mechanosensitive currents observed in their native environment (10). Thus, other mechanically activated channels in addition to TRPs and ASICs could also sense stretch stimuli in the bladder urothelium.

* This work was supported by Grants-in-Aid for Scientific Research 24791640 (to T. Miyamoto), 23592361 (to T. Mochizuki), 23390381 (to M. Takeda), and 23249012 (to M. Tominaga) from the Ministry of Education, Culture, Sports, Science, and Technology of Japan.
[1] To whom correspondence may be addressed. Tel.: 81-552-73-9643; Fax: 81-552-73-9659; E-mail: tsutomu@yamanashi.ac.jp.
[2] To whom correspondence may be addressed: Division of Cell Signaling, Okazaki Institute for Integrative Bioscience, National Institutes of Natural Sciences, Higashiyama 5-1, Myodaiji, Okazaki, Aichi 444-8787, Japan. Tel.: 81-564-59-5286; Fax: 81-564-59-5285; E-mail: tominaga@nips.ac.jp.

[3] The abbreviations used are: SAC, stretch-activated channel; TRP, transient receptor potential; TRPV4, TRP vanilloid 4; KD, knockdown; GSK, GSK1016790A.

True SACs are conserved and present in bacteria, yeast, and plants (27). Although large conductance mechanosensitive channels function as SACs in bacteria (28), mammalian SACs have not been well described. Whereas TRPV4 and two-pore domain K^+ channels are reportedly gated by mechanical stimuli (17, 25, 29, 30), the mechanism through which the cell senses mechanical stimulation remains poorly understood. Recently, Coste *et al.* (31) reported a novel family of mechanically activated cation channels, consisting of Piezo1 and Piezo2 (also called Fam 38A and Fam 38B, respectively) in mammals. These channels have most of the properties of real SACs as described above. Piezo ion channels, first identified in the Neuro2A mouse cell line, are members of a new family of mechanosensitive ion channels found in higher eukaryotic cells. Moreover, they are associated with the physiological response to touch, pressure, and stretch. These channels are ~2500 amino acids long and contain 24–32 transmembrane regions. It appears that they do not require any additional proteins for their opening, and therefore they could directly sense lipid membrane extension (32, 33). Piezo1 currents are similar to those of Piezo2 but have quantitatively different kinetics and conductance. Piezo2 is inactivated more rapidly than Piezo1 and is present in somatosensory neurons. Piezo proteins are also expressed in the mouse lung, colon, and bladder (31). Therefore, we studied whether Piezo1 mediated stretch-evoked Ca^{2+} influx and ATP release in mouse primary urothelial culture cells. We found that Piezo1 is present in the mouse and human bladder urothelium and has a functional role in stretch-evoked Ca^{2+} influx and ATP release in mouse urothelial cells *in vitro*. Additionally, we examined differences between Piezo1 and TRPV4 channels, the latter of which is involved in mechanosensation in the urothelium (26). Finally, we examined the effects of GsMTx4, a peptide isolated from the venom of the tarantula spider. GsMTx4 is widely used to study mechanically activated channels (32, 34, 35) upon stretch stimulation of the urothelium because it inhibits Piezo1 (36).

EXPERIMENTAL PROCEDURES

Animals—Wild-type (C57BL/6Cr) mice and TRPV4-knockout mice (37) backcrossed on a C57BL/6Cr background were used. All experiments were performed with 8–12-week-old male mice. All procedures were conducted in accordance with the Guiding Principles in the Care and Use of Animals in the Field of the Physiologic Society of Japan and the policies of the Institutional Animal Care and Use Committee of the University of Yamanashi (Chuo, Yamanashi, Japan).

Human Subjects—Bladder specimens were harvested from 29 patients with prostate cancer or benign prostatic hyperplasia who had undergone surgery at a single medical hospital (Kawahara Kidney-Urology Clinic, Kagoshima, Japan). This study was approved by the institutional review board of the Kawahara Kidney-Urology Clinic and was conducted according to the principles of the Declaration of Helsinki. All samples were collected with informed consent from the patients.

Preparation of Primary Urothelial Cell Cultures—Whole bladders were removed from anesthetized mice, and urothelial cells were prepared by methods described previously (26), with slight modifications. The bladder was incubated with papain (9.2 units/ml) for 25 min in a water bath at 37 °C. The dissociated and isolated urothelial cells were seeded on elastic silicone chambers (STB-CH-04, STREX, Osaka, Japan) or 8-well chambers (Fisher) coated with fibronectin (AGC Techno Glass Co., Ltd., Shizuoka, Japan) and cultivated in urothelium-dedicated culture medium (CNT-16, CELLnTEC, Bern, Switzerland). All experiments with primary urothelial cell cultures were performed after the cells had formed clusters, which occurred after 72–84 h of cultivation.

TABLE 1
Primers for real-time RT-PCR

Gene	Primer
Human *PIEZO1*	Forward: TGAAGCGGGAGCTCTACAAC
	Reverse: TCTCGTTGGCATACTCCACA
Human *β-ACTIN*	Forward: GGACTTCGAGCAAGAGATGG
	Reverse: AGCACTGTGTTGGCGTACAG
Human *TRPV4*	Forward: GACGGGGACCTATAGCATCA
	Reverse: AACAGGTCCAGGAGGAAGGT
Mouse *Piezo1*	Forward: ATCCTGCTGTATGGGCTGAC
	Reverse: AAGGGTAGCGTGTGTGTTCC
Mouse *Piezo2*	Forward: CGCTCAGAAATGGTGTGCTA
	Reverse: AGATCAAGATGGGCAACAGG
Mouse *Trpv4*	Forward: TCACCTTCGTGCTCCTGTTG
	Reverse: AGATGTGCTTGCTCTCCTTG
Mouse *Gapdh*	Forward: CACAATTTCCATCCCAGACC
	Reverse: GTGGGTGCAGCGAACTTTAT

Quantitative Real-time Reverse Transcription Polymerase Chain Reaction (RT-PCR) Assay—Quantitative real-time RT-PCR assays were performed as reported previously (38). The primer sequences used are shown in Table 1.

In Situ Hybridization Analysis—Mice were anesthetized, and the bladder was removed and frozen with OCT compound (Sakura Finetek, Tokyo, Japan). The frozen tissue was cut on a cryostat and mounted on glass slides. Slides were incubated in PBS with 4% paraformaldehyde. The mouse bladder sections were treated with anti-digoxigenin-AP Fab fragments (1:1000; Roche Applied Science) with blocking reagent. Sense and antisense RNA probes were created from the plasmid constructs of mouse Piezo1 cDNA inserted into pCR2.1 (Invitrogen) and were synthesized by using the digoxigenin RNA labeling kit (Roche Applied Science). Mouse Piezo1 plasmids were linearized with BamHI, and cRNA probes were transcribed from a fragment containing 499 bp (nucleotides 7409–7908, NM_001037298). Digoxigenin labeling was confirmed by the dot blot method.

Immunofluorescence Staining—For immunohistochemistry, whole bladder samples excised from mouse and human specimens were embedded with tissue-TEK OCT compound and frozen in liquid nitrogen. Cryostat sections (10 μm) mounted on glass slides were fixed with 4% paraformaldehyde. The samples were incubated with the primary antibody (rabbit anti-Piezo1 antibodies (Proteintech, Chicago, IL), 1:400) and then covered with the secondary antibody (Alexa Rb488 and Ms546, Molecular Probes, Inc.). For immunocytochemistry, primary urothelial cell cultures were seeded on fibronectin-coated 8-well chambers at a density of 5.0×10^4 cells/well. Primary urothelial cell cultures were incubated with the primary antibodies (rabbit anti-Piezo1 antibodies, 1:100; mouse anti-cytokeratin-7 antibodies, 1:25) and subsequently incubated with the secondary antibodies (Alexa Rb488 and Ms546 (Molecular Probes, Inc.) and DAPI). Immunofluorescence images were

obtained with a confocal laser microscope (Fluoview 1000, Olympus, Tokyo, Japan), as described previously (39). For the comparison of double-stained patterns, images were processed with Photoshop version 5 (Adobe Systems, Mountain View, CA).

Piezo1 siRNA Treatment—siRNA against mouse Piezo1 was used as reported previously (target sequence, TCGGCGCTTGCTAGAACTTCA) (31). Primary urothelial cells were prepared as described above; after 3 h of culture, urothelial cells were transfected with 10 nM siRNAs by using Lipofectamine RNAi MAX (Invitrogen). The culture medium was exchanged 48 h after transfection. The expression of mRNA was measured by quantitative real-time RT-PCR after 72 h of cultivation, and Western blotting was performed after 84 h of cultivation. Mechanical stretch experiments were performed after 72–84 h of cultivation.

Immunoblot Analysis—After transfection with control or *Piezo1* siRNA, primary urothelial cells were lysed in radioimmunoprecipitation assay buffer (Takara, Ootsu, Japan), and lysates were subjected to SDS-PAGE on 7.5% gels by using a Power Station 1000VC system at 20 mA for 120 min. The membranes were incubated with mouse anti-Piezo1 antibodies (1:1000; Proteintech) and mouse anti-β actin antibodies (1:5000) diluted with Can Get Signal® solution 1 (TOYOBO, Osaka, Japan). The proteins were visualized as bands by chemiluminescence (ECL Advance Western blotting Detection Kit, GE Life Sciences).

Direct Mechanical Cell Stretch Experiment and Hypotonicity Cell Swelling Examination—The mechanical stretch experiments were conducted as described previously (26). An elastic silicone chamber (STB-CH-04, STREX) was attached to two pieces of coverglass by an adhesive agent, in which a 1,000-μm-wide slit (from glass edge to edge) was formed in the center of the observation area. This customized design enabled only part of the chamber to be extended upon stretching. Chambers were attached to an extension device (modified version of STB-150, STREX) on the microscope stage. Stretch stimulation was applied using preset stretch speed and distance. A stretch distance of 100–300 μm theoretically induces 10–30% elongation (strain) of the 1,000-μm-wide slit in the silicone chamber, but the actual extents of cell elongation in the chamber were 9.2 $\pm$ 0.7% at 100 μm, 17.5 $\pm$ 1.8% at 200 μm, and 25.5 $\pm$ 2.1% at 300 μm. Upon comparing multiple speeds, we found that significant differences in the changes of intracellular Ca^{2+} concentrations, $[Ca^{2+}]_i$, were most clearly seen at a speed of 100 μm/s.

In the hypotonicity-induced cell swelling examination, hypotonic swelling with 60% of normal osmolarity (340 mOSM) was achieved by adding distilled water in equal volume to the bath solution. The isotonic solution was prepared by adding mannitol.

Measurement of Intracellular Ca^{2+} Concentrations—Intracellular Ca^{2+} concentrations were measured as reported previously (26). Primary urothelial culture cells were loaded with the fluorescent Ca^{2+} indicator fura-2 AM (Invitrogen). The fura-2 fluorescence was measured in a standard bath solution containing 150 mM NaCl, 5 mM KCl, 1.8 mM $CaCl_2$, 1.2 mM $MgCl_2$, 25 mM HEPES, and 10 mM glucose, pH 7.4, adjusted with NaOH. Chemical stimulants were applied directly to the chamber. Ionomycin (5 μM; Sigma-Aldrich) was applied at the final step in each experiment for normalization and to check cell viability. $[Ca^{2+}]_i$ values were measured by ratiometric imaging with fura-2 at 340 and 380 nm, and the emitted light signal was read at 510 nm. F_{340}/F_{380} was acquired and calculated with an imaging processing system (Aquacosmos version 2.6, Hamamatsu Photonics, Hamamatsu, Japan). Changes in ratios (Δ) were calculated by subtracting basal values from peak values.

Photon Imaging of ATP Release—Photon imaging of ATP release was performed as reported previously (40). Stretch-induced ATP release from primary urothelial cell cultures was detected with a luciferin-luciferase bioluminescence assay (ATP bioluminescence assay kit CLS II, Roche Applied Science) and visualized with a VIM camera (C2400-35; Hamamatsu Photonics) by using an integration time of 30 s. The absolute ATP concentration was estimated by using a standard ATP solution (Roche Applied Science). The standard calibration curve yielded a correlation coefficient for bioluminescence *versus* ATP concentration of 0.9917 over a concentration range of 0 nM to 10.0 μM. Data were imaged with Aquacosmos software (Hamamatsu Photonics) and analyzed with ImageJ 1.41 software (National Institutes of Health).

Whole-cell Patch Clamp Recording for HEK293 Cells Overexpressing TRPV4—Human embryonic kidney-derived 293 (HEK293) T cells were maintained in Dulbecco's modified Eagle's medium (WAKO Pure Chemical Industries, Ltd., Osaka, Japan), and cells were transfected with 1.0 μg of mouse TRPV4 plasmid by using Lipofectamine Plus reagent (Invitrogen). Whole-cell patch clamp recordings were performed 24 h after transfection. HEK293 cells on coverslips were mounted in a chamber and superfused with the standard bath solution that was used in the Ca^{2+} imaging experiments. The pipette solution contained 140 mM KCl, 5 mM EGTA, and 10 mM HEPES, pH 7.4. Data were sampled at 10 kHz and filtered at 4 kHz for analysis (Axon 700B amplifier with pCLAMP software, Axon Instruments, Molecular Devices, Tokyo, Japan). Membrane potential was clamped at -60 mV, and voltage ramp pulses from -100 to $+100$ mV (500 ms) were applied every 5 s. GsMTx4 (100 μl/min) was applied via another pipette close to the recorded cell. All experiments were performed at room temperature.

Statistical Analyses—The experimental results were expressed as means $\pm$ S.E. The statistical significance of differences between two groups was determined by Student's *t* test. The statistical significance for multiple comparisons was determined by using the Tukey-Kramer analysis method. *p* values of <0.05 were considered statistically significant.

RESULTS

Expression of Piezo1 in the Mouse Urothelium—Piezo1 is highly expressed in the mouse lung tissue and the urinary bladder (31). To confirm the distribution of *Piezo1* and *Piezo2*, we examined *Piezo1 and Piezo2* mRNA expression levels in various organs, including the urinary tract tissues. Real-time RT-PCR analyses revealed abundant *Piezo1* mRNA expression in the mouse urinary tract, especially in the bladder (Fig. 1*A*). To examine the localization of *Piezo1* in the mouse bladder, we performed *in situ* hybridization. The *Piezo1* signals were pre-

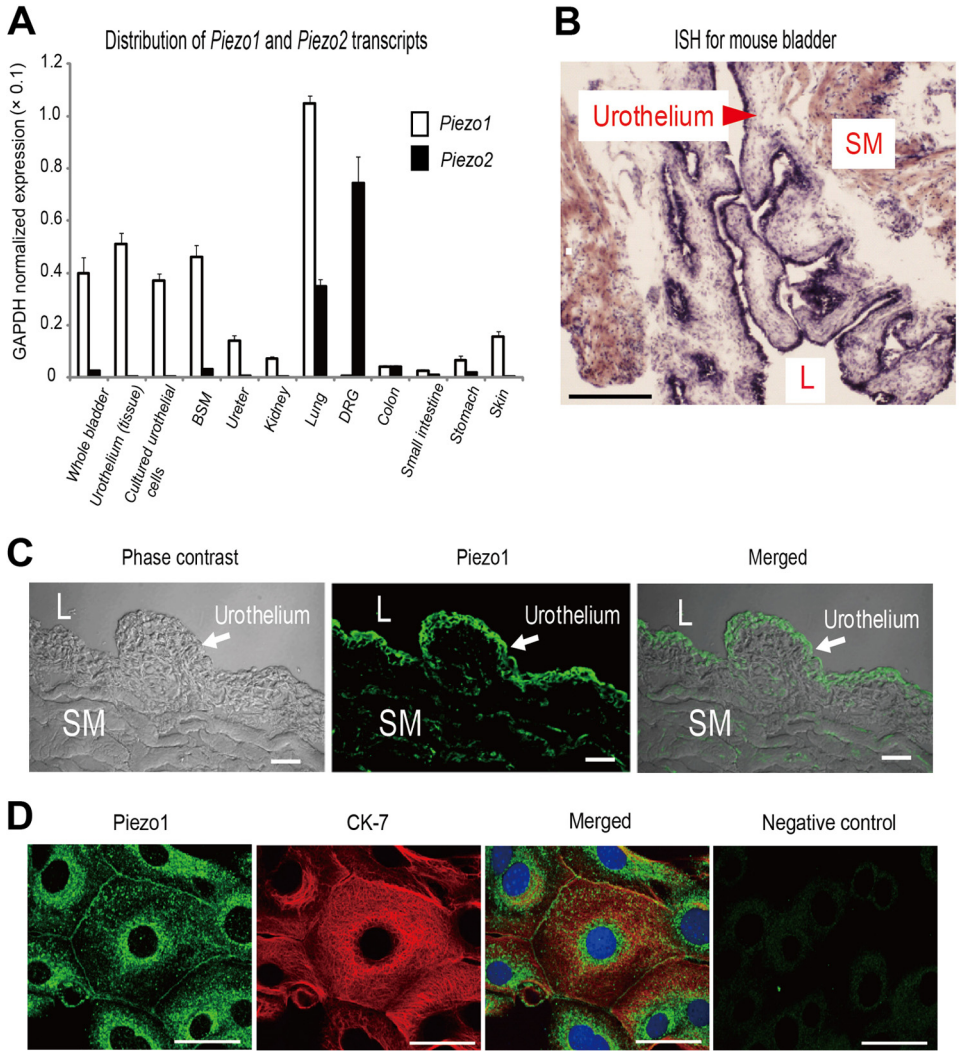

FIGURE 1. **Expression of *Piezo1* mRNA and Piezo1 protein in mouse urothelium.** *A*, quantitative real-time RT-PCR analysis of *Piezo1* and *Piezo2* mRNA expression in tissues and cells, including urinary tract organs. Glyceraldehyde-3-phosphate dehydrogenase (*GAPDH*) was used as the reference gene. *White bars* and *black bars*, *Piezo1* and *Piezo2*, respectively. *BSM*, bladder smooth muscle; *DRG*, dorsal root ganglion. Data are presented as means ± S.E. *B*, *in situ* hybridization (ISH) analysis of *Piezo1* expression in mouse bladder. An *arrowhead* indicates the urothelial layer. *SM*, smooth muscle; *L*, lumen; *scale bar*, 500 μm. *C*, Piezo1-like immunoreactivity in the mouse bladder. *Scale bars*, 100 μm. *D*, expression of Piezo1 (*green*) and cytokeratin-7 (*CK-7*) (*red*), a urothelium marker, in cultured primary mouse urothelial cells. The *far right panel* indicates that no Piezo1-like immunoreactivity was detected in cells by an anti-Piezo1 antibody preincubated with antigenic peptide. *Blue*, DAPI. *Scale bars*, 20 μm.

dominantly found in the urothelial layer rather than the smooth muscle layer (Fig. 1*B*). In contrast, little *Piezo2* expression was detected in the urinary tract tissues (Fig. 1*A*). Thus, we focused on Piezo1 expressed in the mouse urothelium.

Next, we performed immunofluorescence assays for Piezo1 in the mouse whole bladder sections and in primary cultured urothelial cells. Immunohistochemistry revealed that Piezo1-like immunoreactivity was mainly observed in the urothelium, with less immunoreactivity in the stromal tissues, including the smooth muscle (Fig. 1*C*). Immunocytochemistry showed that Piezo1-like immunoreactivity occurred at the plasma membrane and cytoplasm near the nucleus, and the expression of cytokeratin-7 (*CK-7*), an intermediate filament protein present in all urothelial layers and considered to be an urothelial marker (41), overlapped well (Fig. 1*D*). The cytoplasmic Piezo1 signals were no longer observed after preincubation of the antibody with a blocking peptide, indicating the specificity of the Piezo1 signals detected by the antibody (Fig. 1*D*, *far right*).

Effects of siRNA-mediated Knockdown of Piezo1 on Primary Urothelial Cultured Cells—To determine the involvement of Piezo1 in the responses to cell swelling or cell stretch stimulation, we treated primary urothelial cultured cells with a *Piezo1*-specific siRNA. This intervention reduced *Piezo1* mRNA levels by ~60%, whereas treatment with control siRNA did not (Fig. 2*A*). Western blotting analyses revealed that *Piezo1* siRNA treatment also suppressed Piezo1 protein expression (Fig. 2*B*).

Electrophysiological investigations have shown that mechanical stretch (application of positive or negative pressure to a patch membrane through a patch pipette) activates cationic currents in HEK293 cells overexpressing Piezo1 (31, 42). Therefore, to determine whether cell swelling stimulation activates Piezo1 channels, we evaluated changes in cytosolic Ca^{2+} concentrations ($[Ca^{2+}]_i$) upon exposure to hypotonic osmolarity in urothelial cells by using a Ca^{2+}-imaging system. $[Ca^{2+}]_i$ increase upon hypotonic stimulus was significantly suppressed in Piezo1-knockdown (KD) cells with siRNA compared with

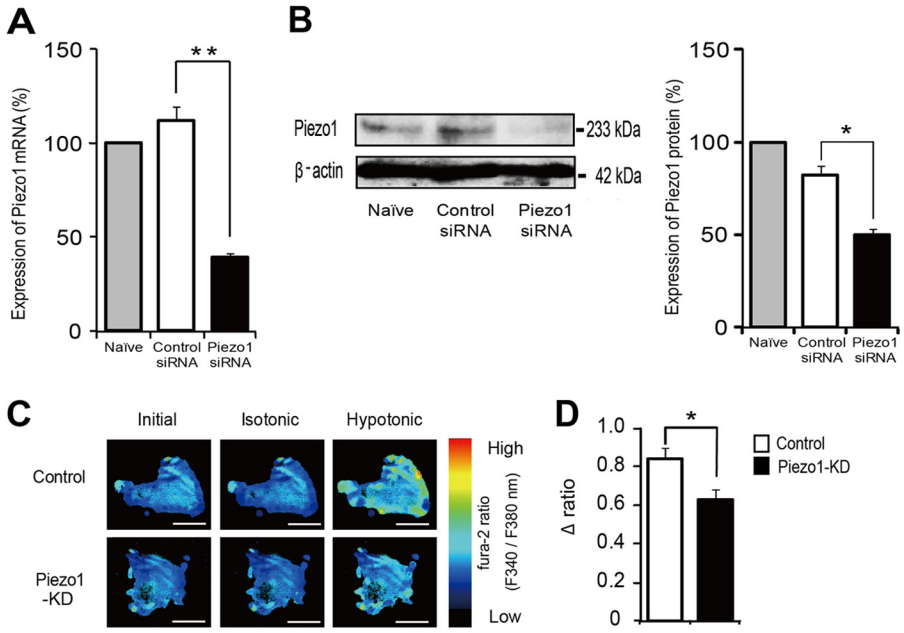

FIGURE 2. **Effects of siRNA-mediated knockdown of Piezo1 on primary urothelial cultured cells.** *A*, quantitative analysis of *Piezo1* mRNA levels by real-time RT-PCR in control mouse primary-cultured urothelial cells (*Naïve*) and cells treated with control siRNA or Piezo1 siRNA. Data are presented as percentage of naive cells ($n = 6$). *B*, detection of Piezo1 protein by immunoblotting in lysates from mouse primary-cultured urothelial cells. Representative gel images (*left*) and analyzed data (*right*) are shown (Piezo1, 233 kDa; β-actin, 42 kDa). Data are presented as percentage of naive cells ($n = 3$). *C*, changes in $[Ca^{2+}]_i$ from control siRNA-treated urothelial cells and Piezo1-KD urothelial cells upon exposure from isotonic (340 mosM) to hypotonic (200 mosM) solution, as indicated by the fura-2 ratio with *pseudocolor* expression. *Scale bars*, 100 μm. *D*, average changes in $[Ca^{2+}]_i$ (difference between base and peak (Δ *ratio*)) by hypotonic stimulation ($n = 12$ experiments (233 cells) for control and 13 experiments (254 cells) for Piezo1-KD). All data are presented as means ± S.E. (*error bars*). *, $p < 0.05$; **, $p < 0.01$, Student's *t* test, as compared with the control.

that of cells treated with control siRNA (Fig. 2, *C* and *D*). These results clearly showed that mouse primary urothelial cell cultures retained functional Piezo1 expression.

Mechanical Stretch Stimulation Evokes Piezo1 Activation in Urothelial Cells—We previously reported that urothelial cells sense mechanical stretch stimuli by using a uniaxial cell extension system. Mechanical stretch stimulation caused Ca^{2+} influx, leading to ATP release in mouse primary urothelial cell cultures (26). Therefore, we investigated whether Piezo1 is involved in $[Ca^{2+}]_i$ changes by direct mechanical stretch stimulation by using a cell extension device and a Ca^{2+}-imaging system. Urothelial cells were cultivated on a stretch silicon chamber, and $[Ca^{2+}]_i$ changes in response to stretch stimulation were examined. Fig. 3*A* demonstrates representative $[Ca^{2+}]_i$ changes with *pseudocolor images* before and after stretch stimulation. Stretch-evoked $[Ca^{2+}]_i$ increases were significantly suppressed in Piezo1 siRNA-treated cells (Piezo1-KD cells) compared with control siRNA-treated cells (Fig. 3, *A* and *B*). Stretch stimulation evoked $[Ca^{2+}]_i$ increases in a stretch distance-dependent manner in urothelial cells (Fig. 3*C*). Because stretch-evoked $[Ca^{2+}]_i$ increases started at a stretch distance of 100 μm (actual extent of cell elongation rate, 9.2 ± 0.7%) and were saturated at 400 μm (cell extension rate, 30.5 ± 2.1%), a stretch distance of 200 μm (cell extension rate, 17.5% ± 1.8%) was chosen for the cell extension system in this experiment. The stretch speed of the cell extension system was fixed at 100 μm/s as explained under "Experimental Procedures." The average peak of $[Ca^{2+}]_i$ increase in response to stretch stimulation was significantly reduced in Piezo1-KD cells in the presence of extracellular Ca^{2+}, and Ca^{2+} responses were small in both cell types in the absence of extracellular Ca^{2+} (Fig. 3*D*), suggesting that Ca^{2+} influx through Piezo1 channels caused $[Ca^{2+}]_i$ increases upon mechanical stretch stimulation in primary urothelial cell cultures.

Stretch-induced ATP Release from Urothelial Cells via Piezo1—Bladder urothelium releases ATP upon stretch stimulation, which mediates signaling to primary afferent neurons via purinergic receptors (43, 44). To determine whether activation of Piezo1 is required for the stretch-induced ATP release from urothelial cells, we measured the amount of extracellular ATP following mechanical cell stretch stimulation by using an ATP photon imaging system. Urothelial cells on a stretch chamber were extended by using the same conditions as in the Ca^{2+}-imaging experiment (stretch distance, 200 μm; stretch speed, 100 μm/s). Upon stretch stimulation, prominent ATP release occurred in control cells, whereas ATP release from Piezo1-KD cells was significantly reduced (Fig. 4, *A* and *B*), which was consistent with the results of the Ca^{2+}-imaging experiment (Fig. 3*D*). The amount of released ATP was suppressed by chelation of extracellular Ca^{2+}, indicating that activation of Piezo1 and the resulting $[Ca^{2+}]_i$ increase were essential for ATP release upon stretch stimulation in primary urothelial cell cultures.

Differences in the Properties of the Piezo1 and TRPV4 Channels—The TRPV4 channel functions as a mechanosensor in mouse primary urothelial cell cultures (26, 43). Therefore, we compared the functions of Piezo1 and TRPV4 channels by measuring stretch-evoked changes in $[Ca^{2+}]_i$. To explore the functional role of these channels, we compared the stretch-evoked changes in $[Ca^{2+}]_i$ in control urothelial cells, Piezo1-KD cells, TRPV4-knock-out (KO) cells, and TRPV4-KO/Piezo1-KD cells with three different stretch lengths (100, 200, and 300 μm). At a 200-μm stretch length, the stretch-evoked

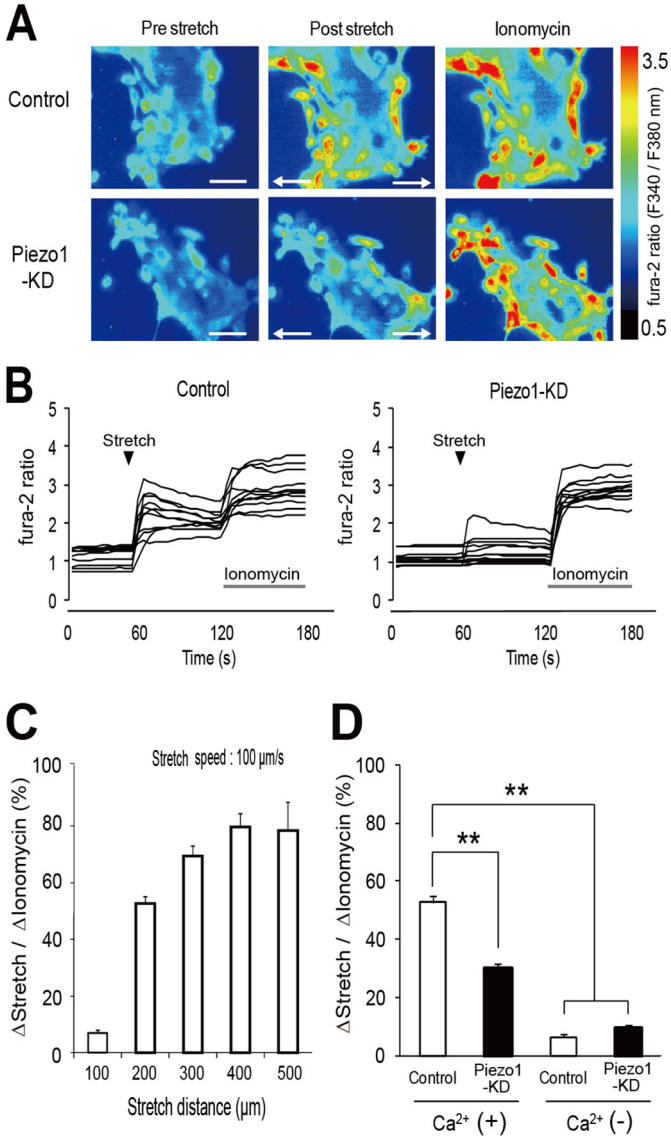

FIGURE 3. **Ca^{2+} responses to mechanical stretch stimulation in mouse primary cultured urothelial cells.** *A*, representative *pseudocolor images* of $[Ca^{2+}]_i$ increase upon stretch stimulation in control siRNA-treated urothelial cells (*top*) and Piezo1-KD cells (*bottom*). Stretch speed was fixed at 100 μm/s, and the distance was 200 μm. Cells were extended transversely (indicated by *arrows*) in both cell types. Ionomycin (5 μM) was applied after stretching. *Scale bars*, 100 μm. *B*, quantification of $[Ca^{2+}]_i$ changes (fura-2 ratio changes) in individual cells. All traces were obtained from the cells shown in *A*. *Black arrowheads* denote the onset of stretch. *Gray bars*, 5 μM ionomycin application. *C*, stretch distance-dependent $[Ca^{2+}]_i$ responses in mouse primary-cultured urothelial cells. $n = 8$ (151 cells), $n = 8$ (168 cells), $n = 8$ (166 cells), $n = 7$ (138 cells), and $n = 7$ experiments (124 cells) for 100-, 200-, 300-, 400-, and 500-μm extension, respectively. The stretch speed was fixed at 100 μm/s. Data are presented as means ± S.E. (*error bars*). *D*, stretch-evoked changes in fura-2 ratio normalized to the ratio changes by 5 μM ionomycin (percentage) in control siRNA-treated urothelial cells (*Control*) and Piezo1-KD cells (*KD*) in the presence (+) or absence (−) of extracellular Ca^{2+}. Data are from eight experiments for each group with 168, 183, 173, and 150 cells for control Ca^{2+}(+), Piezo1-KD Ca^{2+}(+), Control Ca^{2+}(−), and Piezo1-KD Ca^{2+}(−), respectively. Data are presented as means ± S.E. **, $p < 0.01$, Tukey-Kramer method.

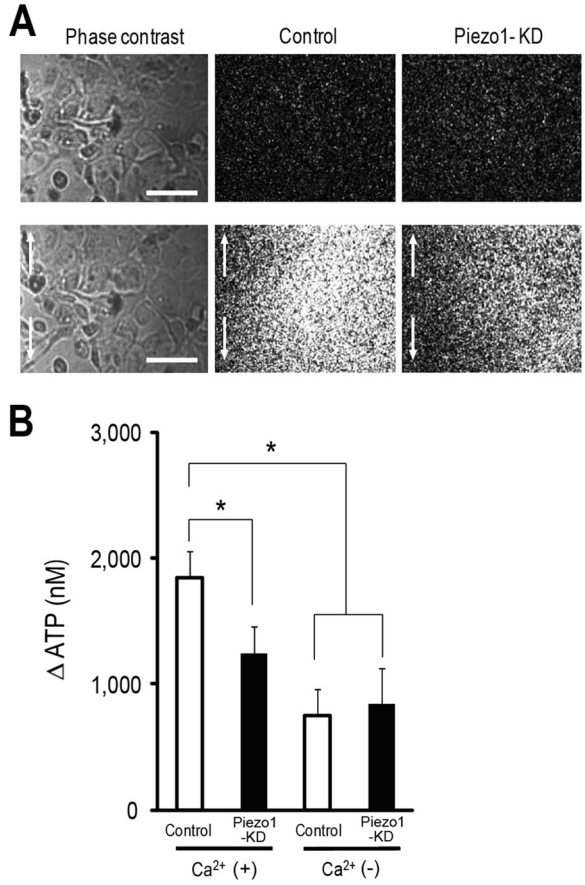

FIGURE 4. **Visualization of stretch-induced ATP release from urothelial cells.** *A*, *left panels* show urothelial cells in phase-contrast images, and the *middle* and *right* panels show photon count images of control cells (*Control*) and Piezo1-KD cells, respectively. The *top* and *bottom* panels show the images before and after mechanical stretch, respectively. Stretch speed was 100 μm/s, and stretch distance was 200 μm. Cells were extended to the *vertical axis* (indicated by *arrows*). *Scale bars*, 100 μm. *B*, average amount of ATP released from control siRNA-treated urothelial cells (*Control*) and Piezo1-KD cells in the presence (+) or absence (−) of extracellular Ca^{2+}. Data are from eight experiments for each group. Data are presented as means ± S.E. (*error bars*). *, $p < 0.01$, Tukey-Kramer method.

$[Ca^{2+}]_i$ increase was significantly suppressed in Piezo1-KD cells, TRPV4-KO cells, and TRPV4-KO/Piezo1-KD cells compared with control cells (Fig. 5*A*). Interestingly, when TRPV4-KO urothelial cells were treated with *Piezo1* siRNA, the stretch-evoked increase in $[Ca^{2+}]_i$ was further suppressed to a level near that observed in the absence of extracellular Ca^{2+} (Fig. 3*D*), suggesting that Piezo1 and TRPV4 contributed to the stretch-induced $[Ca^{2+}]_i$ increases in primary mouse urothelial cells. At a 100-μm stretch length, the stretch-evoked $[Ca^{2+}]_i$ increases in Piezo1-KD cells and TRPV4-KO/Piezo1-KD cells were significantly lower than that in control cells, but the $[Ca^{2+}]_i$ increase in TRPV4-KO cells was not significantly different from that in control cells. In contrast, at a 300-μm stretch length, stretch-evoked $[Ca^{2+}]_i$ increases were not significantly different among the four cell types, probably due to saturation of the mechanisms causing $[Ca^{2+}]_i$ increases. These results indicate that Piezo1 senses stretch stimulation over a wider range than the TRPV4 channel and that the sensitivity of Piezo1 to stretch stimulation is higher than that of TRPV4.

Next, we compared the amount of ATP release from each cell type upon stretch stimulation with the same conditions as in the Ca^{2+}-imaging experiments. At a 200-μm stretch length, stretch-induced ATP release from Piezo1-KD and TRPV4-KO/Piezo1-KD cells was significantly reduced compared with control cells. At a 100-μm stretch length, small amounts of ATP

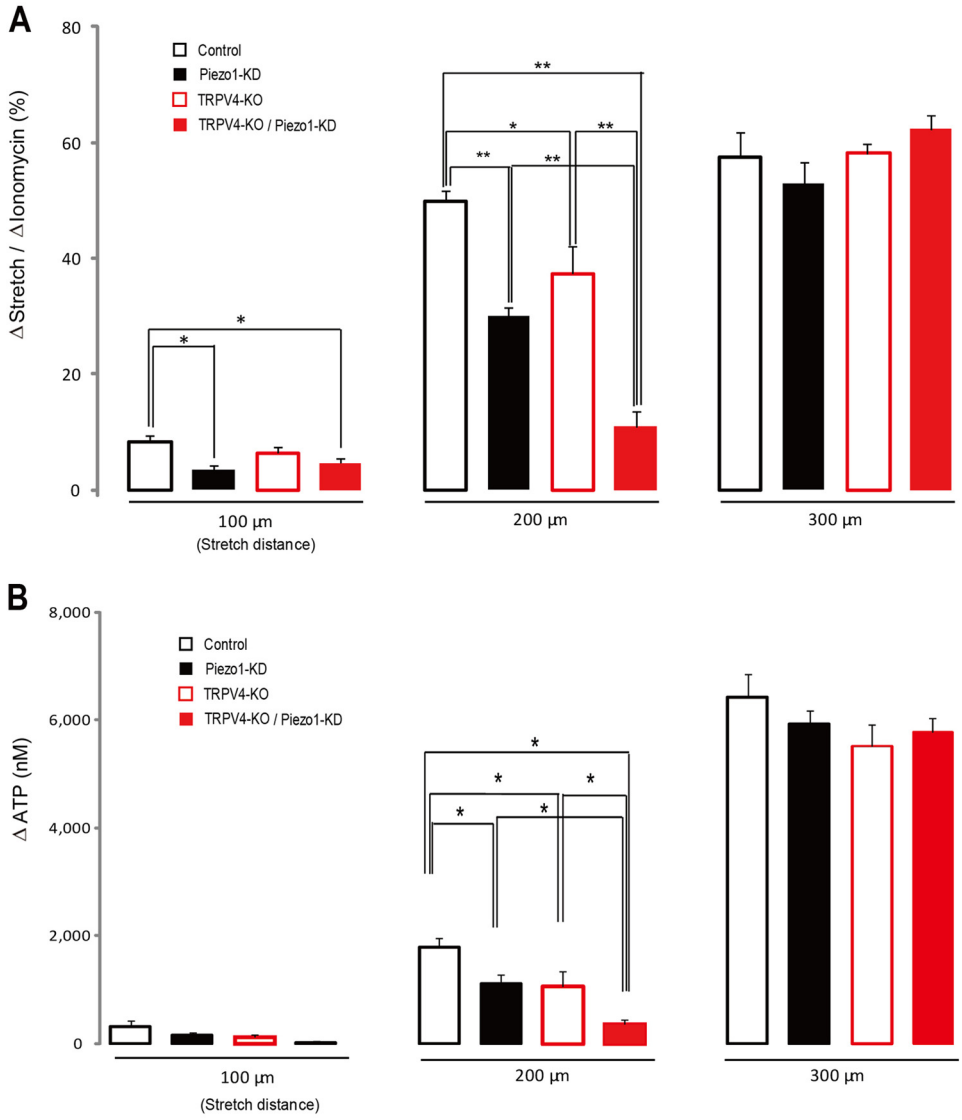

FIGURE 5. **Different functional properties between Piezo1 and TRPV4 channels.** *A*, $[Ca^{2+}]_i$ responses (normalized to ionomycin responses) in mouse primary-cultured urothelial cells at different stretch distances (100, 200, and 300 μm) in control siRNA-treated urothelial cells obtained from wild type mice (*Control*), Piezo1 siRNA-treated cells from wild type mice (*Piezo1-KD*), control siRNA-treated urothelial cells from TRPV4 knock-out mice (*TRPV4-KO*) and Piezo1 siRNA-treated cells from TRPV4 knock-out mice (*TRPV4-KO/Piezo1-KD*). *B*, comparison of stretch-induced ATP release from mouse primary-cultured urothelial cells at different stretch distances (100, 200, and 300 μm) in control, Piezo1-KD, TRPV4-KO, and TRPV4-KO/Piezo1-KD cells. Data are from eight experiments for each group for both $[Ca^{2+}]_i$ responses and ATP release. Cell numbers examined for $[Ca^{2+}]_i$ responses were 151 cells (100 μm), 168 cells (200 μm), and 166 cells (300 μm) for control; 201 cells (100 μm), 183 cells (200 μm), and 187 cells (300 μm) for Piezo1-KD; 149 cells (100 μm), 122 cells (200 μm), and 202 cells (300 μm) for TRPV4-KO; and 160 cells (100 μm), 131 cells (200 μm), and 212 cells (300 μm) for TRPV4-KO/Piezo1-KD. All data are presented as means ± S.E. (*error bars*). *, $p < 0.05$; **, $p < 0.01$, Tukey-Kramer method.

were released from all cell types without significant differences, probably because $[Ca^{2+}]_i$ increases under these conditions were not sufficient to cause ATP releases. At a 300-μm stretch length, large amounts of ATP were released from all the four cell types with no significant differences (Fig. 5*B*) similar to the $[Ca^{2+}]_i$ increase (Fig. 5*A*). Collectively, these results suggested that activation of both Piezo1 and TRPV4 and the resultant $[Ca^{2+}]_i$ increase critically contributed to ATP release upon stretch stimulation (at least under the 200-μm stretch length) in primary urothelial cell cultures.

GsMTx4 Inhibited Piezo1 in Mouse Urothelial Cells—Bae *et al.* (36) previously reported that extracellular GsMTx4 (3–5 μM) inhibited mechanical stimulus-evoked currents by ~80% in outside-out patches using HEK293 cells overexpressing Piezo1. Therefore, we evaluated the effects of GsMTx4 in stretch experiments, examining the dose-dependent effects of GsMTx4 in our urothelial cell stretch study. In control urothelial cells, GsMTx4 significantly attenuated the stretch-evoked $[Ca^{2+}]_i$ increase to a level observed in Piezo1-KD cells at concentrations greater than 10 μM. In contrast, GsMTx4 failed to affect the stretch-evoked $[Ca^{2+}]_i$ increase in Piezo1-KD cells (Fig. 6*A*), suggesting that the GsMTx4-dependent component could be attributed to Piezo1. Stretch-induced ATP release was also inhibited by application of GsMTx4 in control urothelial cells (Fig. 6*B*). Taken together, these data suggested that inhibition of Piezo1 by GsMTx4 suppressed the resulting increase in $[Ca^{2+}]_i$, and this suppression was essential to the reduction in ATP release upon stretch stimulation in primary urothelial

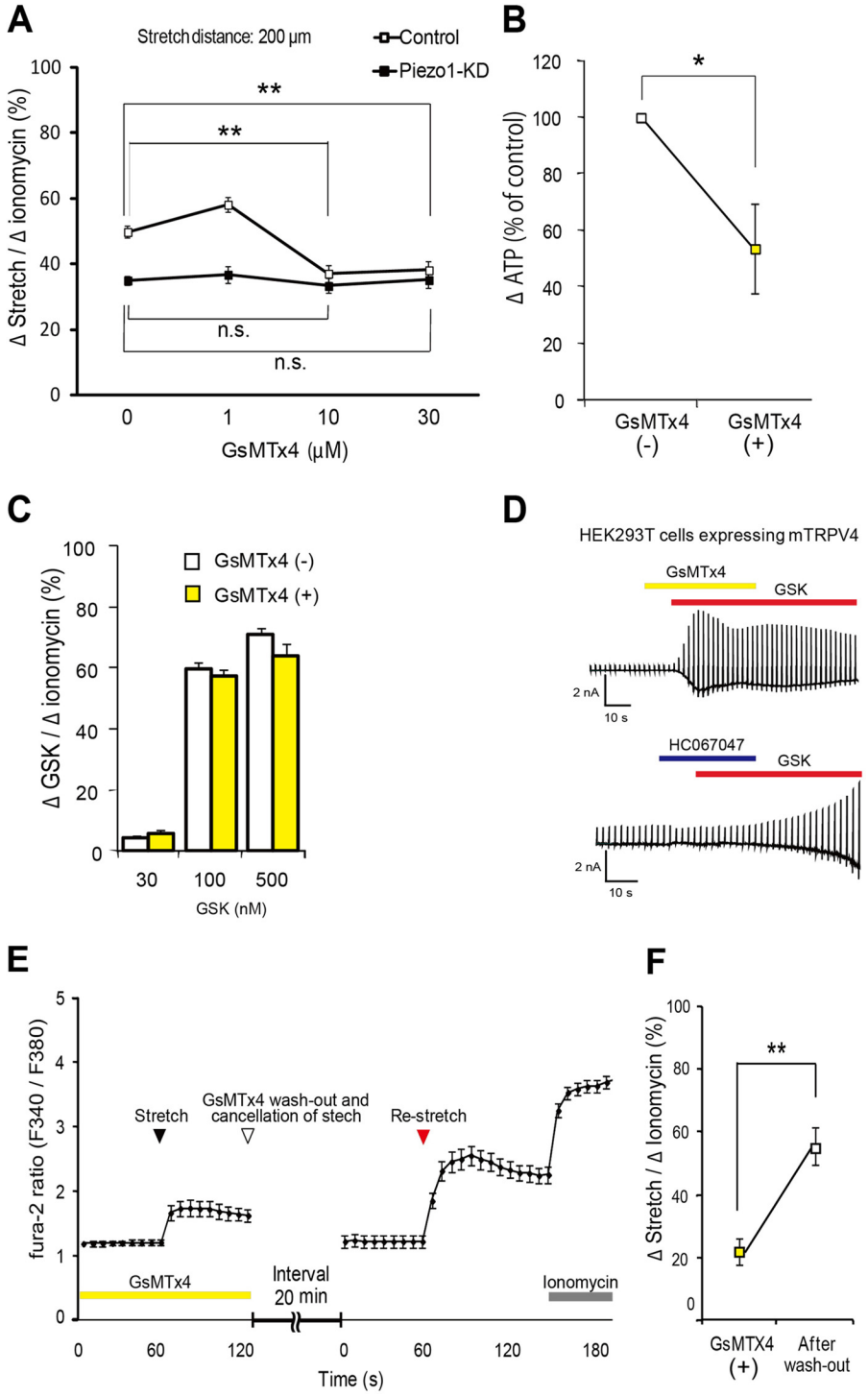

FIGURE 6. **Inhibitory effects of GsMTx4 for Piezo1 in the urothelial cells.** *A*, concentration-dependent inhibition of stretch-evoked $[Ca^{2+}]_i$ responses by GsMTx4 in control siRNA-treated urothelial cells (*Control*) and Piezo1-KD cells. The stretch speed and stretch distance were 100 μm/s and 200 μm. Data were from 7 (control/Piezo1-KD), 10/10, 12/10, and 10/10 experiments for 0, 1, 10, and 30 μM GsMTx4, respectively. Cell numbers were 140/152 (control/Piezo1-KD), 199/202, 233/201, and 178/188 for 0, 1, 10, and 30 μM, respectively. Data are presented as means ± S.E. (*error bars*). *, $p < 0.05$; **, $p < 0.01$, Student's *t* test. *n.s.*, not significant. *B*, effects of GsMTx4 (10 μM) on the stretch-evoked ATP release from urothelial naive cells. The stretch distance was 200 μm. Data were from 13 and 14 experiments for GsMTx4(−) and GsMTx4(+), respectively, and are presented as percentage of control and means ± S.E. *, $p < 0.05$, Student's *t* test. *C*, GSK-evoked $[Ca^{2+}]_i$ increases (normalized to ionomycin responses) at different concentrations in urothelial cell cultures with (+) or without (−) GsMTx4. Data were from five experiments for all groups. Cell numbers were 92/81 (without/with GsMTx4 treatment), 132/89, and 130/145 for 30, 100, and 500 nM GsMTx4, respectively. *D*, representative traces of GSK (100 nM)-evoked TRPV4 currents in the presence of GsMTx4 (10 μM) (*top*) or HC067047 (a TRPV4-selective antagonist; 10 μM) (*bottom*). *Yellow*, *red*, and *blue bars* indicate application of GsMTx4, GSK, and HC067047, respectively. *E*, reversible effects of GsMTx4 (10 μM) on the stretch-evoked $[Ca^{2+}]_i$ increases in mouse primary-cultured urothelial cells. The first stretch stimulus was applied (*black arrowhead*) in the presence of GsMTx4 (*yellow bar*), and GsMTx4 was washed out, and the stretch was halted (a *white arrowhead*). The cells were then restretched (a *red arrowhead*) after a 20-min interval in the absence of GsMTx4. The first stretch and restretch stimulations were applied under the same conditions (stretch speed and distance are 100 μm/s and 200 μm, respectively). 5 μM ionomycin was applied to confirm cell viability (*gray bar*). Data were from 20 experiments (366 cells). *F*, comparison of the stretch-evoked $[Ca^{2+}]_i$ increases (normalized to ionomycin responses) in the GsMTx4 treatment and after its wash out. **, $p < 0.01$, Student's *t* test.

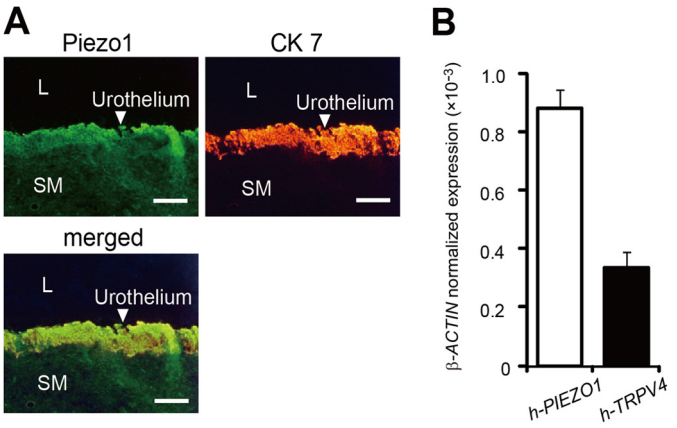

FIGURE 7. **Piezo1 expression in human bladder.** *A*, Piezo1-like and cytokeratin-7 (*CK 7*) immunoreactivity in the urothelial cell layer of human bladder. *White arrowheads*, urothelium. *SM*, smooth muscle; *L*, lumen. *Scale bar*, 100 μm. *B*, expression levels of *PIEZO1* and *TRPV4* mRNAs (normalized to *β-ACTIN*) in the human bladder urothelium determined by quantitative RT-PCR. Data are presented as means ± S.E. (*error bars*).

cell cultures. To rule out the possibility that GsMTx4 inhibits TRPV4 channel activity, we examined the $[Ca^{2+}]_i$ response to GSK1016790A (GSK), a TRPV4-selective agonist (45), in urothelial cells. GSK evoked a prominent increase in $[Ca^{2+}]_i$ in a dose-dependent manner, but the Ca^{2+} response to GSK was not affected by GsMTx4 treatment at any of the tested GSK concentrations (Fig. 6*C*). Moreover, we performed a whole-cell patch clamp recording to examine whether GsMTx4 inhibits the GSK-evoked current in HEK293T cells expressing mouse TRPV4. In this experiment, we also confirmed that GsMTx4 did not inhibit TRPV4 activity, whereas HC067047, a specific TRPV4 inhibitor, almost completely blocked the TRPV4 activity (Fig. 6*D*).

Next, to determine whether the inhibitory effect of GsMTx4 was reversible, we performed a GsMTx4 wash-out study upon stretch stimulation. In the mechanical stretch experiment, the stretch-evoked $[Ca^{2+}]_i$ increase was relatively small in the presence of GsMTx4, and it became larger after wash-out of GsMTx4 (Fig. 6, *E* and *F*), approaching the level in the control cells (Fig. 5*A*). These results indicated that inhibition of Piezo1 by GsMTx4 was reversible upon mechanical stretch stimulation in urothelial cells.

Human Piezo1 Is Highly Expressed in the Human Bladder Urothelium—Finally, to confirm the expression of Piezo1 in the human bladder, we performed immunohistochemical analysis with human bladder specimens. We found that Piezo1-like immunoreactivity was mainly present in the urothelium layer (Fig. 7*A*), which is consistent with the findings in the mouse bladder (Fig. 1*C*). Moreover, we examined the expression of human *PIEZO1* and human *TRPV4* mRNAs in the human bladder urothelium by quantitative RT-PCR. Fig. 7*B* shows that *PIEZO1* mRNA was much more abundant than *TRPV4* mRNA in the human urothelium. These results suggested that Piezo1 might be more important than TRPV4 for detecting urothelial extension during bladder distention in humans.

DISCUSSION

The present study provides evidence that the Piezo1 channel is involved in mechanosensory transduction in the urinary bladder. First, we demonstrated that Piezo1 was predominantly present in the mouse urothelium, and Piezo1 expression was also confirmed in mouse primary urothelial cell cultures (Fig. 1). Second, we demonstrated that mechanical stretch stimulation of urothelial cells activated Piezo1, leading to $[Ca^{2+}]_i$ increases and ATP release in primary urothelial cell cultures (Figs. 2–5). Third, we showed that GsMTx4 attenuated the stretch-evoked $[Ca^{2+}]_i$ increase and ATP release by urothelial cells (Fig. 6). Finally, we showed that Piezo1 was highly expressed in the human bladder urothelium (Fig. 7). These findings indicate that Piezo1 plays a crucial role in sensing mechanical force in the urothelium and participates in the mechanosensory-transduction pathway in the urinary bladder. To the best of our knowledge, this is the first study to reveal the expression of Piezo1 in the bladder urothelium and to describe the function of Piezo1 upon mechanical stretch stimulation in primary urothelial cell cultures.

In our immunocytochemical study, Piezo1 expression was detected in the plasma membrane and cytoplasm near the nucleus in mouse urothelial cell cultures (Fig. 1*D*), data that are consistent with previous reports (31, 46). Piezo1 expression in the plasma membrane is consistent with its function as a SAC that mediates Ca^{2+} influx.

We previously found that TRPV4 is responsible for sensing mechanical stretch and causing Ca^{2+} entry into urothelial cells (26). Therefore, in the present study, we compared the functional roles of Piezo1 and TRPV4 channels between urothelial cells obtained from TRPV4-KO mice with and without *Piezo1* siRNA treatment. At a 200-μm stretch length, the stretch-evoked $[Ca^{2+}]_i$ increase was strongly suppressed almost to control cell levels in the absence of extracellular Ca^{2+} when *Piezo1* mRNA was knocked down in TRPV4-KO cells (Figs. 3*D* and 5*A*). These findings indicate that Piezo1 and TRPV4 are activated independently and that the stretch-evoked Ca^{2+} influx pathway is mediated mainly through Piezo1 and TRPV4 channels. In contrast, at a 100-μm stretch length, stretch-evoked Ca^{2+} influx in Piezo1-KD cells was significantly lower than that in control cells, whereas that in TRPV4-KO cells was not significantly different from that in control cells (Fig. 5*A*). These findings imply that urothelial cells might recognize and distinguish the different intensity of mechanical force by using different mechanosensors. The sensitivity of Piezo1 for stretch stimulation was higher than that of TRPV4, and Piezo1 might be a more sensitive mechanosensor than TRPV4. This heightened sensitivity might be related to the fact that Piezo1 does not require any other proteins for its activation and could be directly activated by membrane stretch (32, 33, 42). In contrast, TRPV4 interacts with the actin cytoskeleton (47) to form a mechanosensory complex (48) and is activated by an endogenous ligand, epoxyeicosatrienoic acid, a metabolite of arachidonic acid, although TRPV4 expressed in *Xenopus* oocytes has been reported to be directly activated by membrane stretch (25).

ATP released from urothelial cells depends on the increase in intracellular Ca^{2+} concentrations (26, 49) and plays an important role for signal transduction to afferent nerve endings; ATP regulates bladder functions, including the micturition reflex and nonvoiding contractions (44). In the present study, the

amount of ATP released from the urothelium paralleled the changes in the cytosolic Ca^{2+} concentrations at a 200-μm stretch length. However, Ca^{2+} influx in Piezo1-KD cells was significantly reduced compared with that in control cells and TRPV4-KO cells at a 100-μm stretch length (Fig. 5*A*), whereas ATP released from urothelial cells was not significantly different among control cells, Piezo1-KD cells, and TRPV4-KO cells (Fig. 5*B*). These results could imply that the small increase in cytosolic Ca^{2+} concentrations at a 100-μm stretch length is not sufficient to cause ATP release. Two mechanisms for ATP release by epithelia have been proposed: a conductive release through ion channels (50, 51) and an exocytotic release with ATP-enriched vesicles (52, 53), which is regulated by intracellular Ca^{2+} concentrations. Ca^{2+} influx via Piezo1 might activate anion channels or connexin hemichannels (54) through which ATP is released. Alternatively, ATP could also be released through vesicular exocytosis by a PI3K-mediated pathway (55–57). Given that Piezo1 constitutes one of the Ca^{2+} influx pathways, its activation could be critical for ATP release upon stretch stimulation, although the mechanism for Piezo1-mediated ATP release remains unclear.

Piezo1 is inhibited by ruthenium red, a nonspecific inhibitor of many cation channels (31); this lack of specificity makes it difficult to use ruthenium red to identify the targets of Piezo1 (33). We used GsMTx4, a peptide isolated from tarantula venom that is a much more specific inhibitor of endogenous cationic SACs (35), to determine the involvement of Piezo1 activity in the stretch-evoked responses. It is likely that GsMTx4 inhibits Piezo1 by acting as a gating modifier that is inserted at the channel-lipid interface and prestresses the channel toward the closed conformation (36). We showed that the stretch-evoked $[Ca^{2+}]_i$ increase in control urothelial cells was significantly attenuated by GsMTx4 to the level of Piezo1-KD cells, suggesting that GsMTx4 acts on the Piezo1 channel more selectively than other SACs. We found that GsMTx4 inhibited Piezo1 channel activity and attenuated the stretch-evoked Ca^{2+} influx and ATP release in urothelial cells, although GsMTx4 might have other targets.

We demonstrated that the effect of GsMTx4 on the stretch-evoked $[Ca^{2+}]_i$ increase was reversible (Fig. 6, *E* and *F*) and that Piezo1 was expressed in both mouse and human urothelium (Fig. 7*A*). Those results suggest that GsMTx4 could be useful for the development of agents to treat diseases involving Piezo1, such as urine storage disorders. In the clinical setting, pathological conditions, such as overactive bladder and interstitial cystitis are considered to be correlated with urothelial pathogenesis (58–60). It has recently been speculated that distension during urine storage stimulates urothelial cells to release various chemical mediators like ATP, prostaglandins, nitric oxide, and acetylcholine, which then transfer signals to afferent nerves or muscle cells. Some abnormalities in this pathway could cause overactive bladder and/or interstitial cystitis. We currently have no evidence showing the involvement of mechanical stretch stimulation in the release of other neurotransmitters (besides ATP), which needs to be explored in the future.

In summary, Piezo1 functions as a mechanosensor and plays an important role in the stretch-evoked Ca^{2+} influx and ATP release in the mouse bladder urothelium. Moreover, GsMTx4 inhibits Piezo1 activity in the urothelium. Based on the findings of our current study, we suggest that Piezo1 is an important regulator of bladder function and that pharmacological inhibition of Piezo1 might improve urine storage disorders. It is possible that the specific inhibition of urothelial Piezo1 with compounds such as GsMTx4 might become a novel therapy for overactive bladder and/or interstitial cystitis.

Acknowledgments—We thank Sachiko Tsuchiya, Mie Kanda, Youichi Shinozaki, and Keisuke Shibata for excellent technical assistance. We greatly appreciate the help of Dr. Kawahara in collecting human samples.

REFERENCES

1. Birder, L. A., and de Groat, W. C. (2007) Mechanisms of disease: involvement of the urothelium in bladder dysfunction. *Nat. Clin. Pract. Urol.* **4,** 46–54
2. Araki, I., Du, S., Kobayashi, H., Sawada, N., Mochizuki, T., Zakoji, H., and Takeda, M. (2008) Roles of mechanosensitive ion channels in bladder sensory transduction and overactive bladder. *Int. J. Urol.* **15,** 681–687
3. Everaerts, W., Gevaert, T., Nilius, B., and De Ridder, D. (2008) On the origin of bladder sensing: Tr(i)ps in urology. *Neurourol. Urodyn.* **27,** 264–273
4. Apodaca, G. (2004) The uroepithelium: not just a passive barrier. *Traffic* **5,** 117–128
5. Birder, L. A. (2005) More than just a barrier: urothelium as a drug target for urinary bladder pain. *Am. J. Physiol. Renal Physiol.* **289,** F489–F495
6. de Groat, W. C. (2004) The urothelium in overactive bladder: passive bystander or active participant? *Urology* **64,** 7–11
7. Cockayne, D. A., Hamilton, S. G., Zhu, Q. M., Dunn, P. M., Zhong, Y., Novakovic, S., Malmberg, A. B., Cain, G., Berson, A., Kassotakis, L., Hedley, L., Lachnit, W. G., Burnstock, G., McMahon, S. B., and Ford, A. P. (2000) Urinary bladder hyporeflexia and reduced pain-related behaviour in P2X3-deficient mice. *Nature* **407,** 1011–1015
8. Nilius, B., and Honoré, E. (2012) Sensing pressure with ion channels. *Trends Neurosci.* **35,** 477–486
9. Chalfie, M. (2009) Neurosensory mechanotransduction. *Nat. Rev. Mol. Cell Biol.* **10,** 44–52
10. Delmas, P., Hao, J., and Rodat-Despoix, L. (2011) Molecular mechanisms of mechanotransduction in mammalian sensory neurons. *Nat. Rev. Neurosci.* **12,** 139–153
11. Lumpkin, E. A., and Caterina, M. J. (2007) Mechanisms of sensory transduction in the skin. *Nature* **445,** 858–865
12. Pedersen, S. F., and Nilius, B. (2007) Transient receptor potential channels in mechanosensing and cell volume regulation. *Methods Enzymol.* **428,** 183–207
13. Sharif-Naeini, R., Dedman, A., Folgering, J. H., Duprat, F., Patel, A., Nilius, B., and Honoré, E. (2008) TRP channels and mechanosensory transduction: insights into the arterial myogenic response. *Pflugers Arch.* **456,** 529–540
14. Patel, A. J., Honoré, E., Maingret, F., Lesage, F., Fink, M., Duprat, F., and Lazdunski, M. (1998) A mammalian two pore domain mechano-gated S-like K^+ channel. *EMBO J.* **17,** 4283–4290
15. Maingret, F., Patel, A. J., Lesage, F., Lazdunski, M., and Honoré, E. (2000) Lysophospholipids open the two-pore domain mechano-gated K^+ channels TREK-1 and TRAAK. *J. Biol. Chem.* **275,** 10128–10133
16. Lesage, F., Terrenoire, C., Romey, G., and Lazdunski, M. (2000) Human TREK2, a 2P domain mechano-sensitive K^+ channel with multiple regulations by polyunsaturated fatty acids, lysophospholipids, and G_s, G_i, and G_q protein-coupled receptors. *J. Biol. Chem.* **275,** 28398–28405
17. Brohawn, S. G., Su, Z., and MacKinnon, R. (2014) Mechanosensitivity is mediated directly by the lipid membrane in TRAAK and TREK1 K^+ channels. *Proc. Natl. Acad. Sci. U.S.A.* **111,** 3614–3619
18. Kim, Y., Bang, H., Gnatenco, C., and Kim, D. (2001) Synergistic interaction and the role of C-terminus in the activation of TRAAK K^+ channels by

pressure, free fatty acids and alkali. *Pflugers Arch.* **442,** 64–72
19. Noël, J., Zimmermann, K., Busserolles, J., Deval, E., Alloui, A., Diochot, S., Guy, N., Borsotto, M., Reeh, P., Eschalier, A., and Lazdunski, M. (2009) The mechano-activated K^+ channels TRAAK and TREK-1 control both warm and cold perception. *EMBO J.* **28,** 1308–1318
20. Waldmann, R., and Lazdunski, M. (1998) H^+-gated cation channels: neuronal acid sensors in the NaC/DEG family of ion channels. *Curr. Opin. Neurobiol.* **8,** 418–424
21. Lingueglia, E. (2007) Acid-sensing ion channels in sensory perception. *J. Biol. Chem.* **282,** 17325–17329
22. Christensen, A. P., and Corey, D. P. (2007) TRP channels in mechanosensation: direct or indirect activation? *Nat. Rev. Neurosci.* **8,** 510–521
23. Damann, N., Voets, T., and Nilius, B. (2008) TRPs in our senses. *Curr. Biol.* **18,** R880–R889
24. Nilius, B., Owsianik, G., Voets, T., and Peters, J. A. (2007) Transient receptor potential cation channels in disease. *Physiol. Rev.* **87,** 165–217
25. Loukin, S., Zhou, X., Su, Z., Saimi, Y., and Kung, C. (2010) Wild-type and brachyolmia-causing mutant TRPV4 channels respond directly to stretch force. *J. Biol. Chem.* **285,** 27176–27181
26. Mochizuki, T., Sokabe, T., Araki, I., Fujishita, K., Shibasaki, K., Uchida, K., Naruse, K., Koizumi, S., Takeda, M., and Tominaga, M. (2009) The TRPV4 cation channel mediates stretch-evoked Ca^{2+} influx and ATP release in primary urothelial cell cultures. *J. Biol. Chem.* **284,** 21257–21264
27. Kung, C. (2005) A possible unifying principle for mechanosensation. *Nature* **436,** 647–654
28. Sukharev, S. I., Blount, P., Martinac, B., Blattner, F. R., and Kung, C. (1994) A large-conductance mechanosensitive channel in *E. coli* encoded by mscL alone. *Nature* **368,** 265–268
29. Honoré, E. (2007) The neuronal background K2P channels: focus on TREK1. *Nat. Rev. Neurosci.* **8,** 251–261
30. Patel, A. J., Lazdunski, M., and Honoré, E. (2001) Lipid and mechano-gated 2P domain K^+ channels. *Curr. Opin. Cell Biol.* **13,** 422–428
31. Coste, B., Mathur, J., Schmidt, M., Earley, T. J., Ranade, S., Petrus, M. J., Dubin, A. E., and Patapoutian, A. (2010) Piezo1 and Piezo2 are essential components of distinct mechanically activated cation channels. *Science* **330,** 55–60
32. Suchyna, T. M., Tape, S. E., Koeppe, R. E., 2nd, Andersen, O. S., Sachs, F., and Gottlieb, P. A. (2004) Bilayer-dependent inhibition of mechanosensitive channels by neuroactive peptide enantiomers. *Nature* **430,** 235–240
33. Gottlieb, P. A., and Sachs, F. (2012) Piezo1: properties of a cation selective mechanical channel. *Channels* **6,** 214–219
34. Escoubas, P., and Rash, L. (2004) Tarantulas: eight-legged pharmacists and combinatorial chemists. *Toxicon* **43,** 555–574
35. Suchyna, T. M., Johnson, J. H., Hamer, K., Leykam, J. F., Gage, D. A., Clemo, H. F., Baumgarten, C. M., and Sachs, F. (2000) Identification of a peptide toxin from *Grammostola spatulata* spider venom that blocks cation-selective stretch-activated channels. *J. Gen. Physiol.* **115,** 583–598
36. Bae, C., Sachs, F., and Gottlieb, P. A. (2011) The mechanosensitive ion channel Piezo1 is inhibited by the peptide GsMTx4. *Biochemistry* **50,** 6295–6300
37. Mizuno, A., Matsumoto, N., Imai, M., and Suzuki, M. (2003) Impaired osmotic sensation in mice lacking TRPV4. *Am. J. Physiol. Cell Physiol.* **285,** C96–C101
38. Du, S., Araki, I., Kobayashi, H., Zakoji, H., Sawada, N., and Takeda, M. (2008) Differential expression profile of cold (TRPA1) and cool (TRPM8) receptors in human urogenital organs. *Urology* **72,** 450–455
39. Shibata, K., Sugawara, T., Fujishita, K., Shinozaki, Y., Matsukawa, T., Suzuki, T., and Koizumi, S. (2011) The astrocyte-targeted therapy by Bushi for the neuropathic pain in mice. *PLoS One* **6,** e23510
40. Koizumi, S., Fujishita, K., Inoue, K., Shigemoto-Mogami, Y., Tsuda, M., and Inoue, K. (2004) Ca^{2+} waves in keratinocytes are transmitted to sensory neurons: the involvement of extracellular ATP and P2Y2 receptor activation. *Biochem. J.* **380,** 329–338
41. Erman, A., Veranic, P., Psenicnik, M., and Jezernik, K. (2006) Superficial cell differentiation during embryonic and postnatal development of mouse urothelium. *Tissue Cell* **38,** 293–301
42. Coste, B., Xiao, B., Santos, J. S., Syeda, R., Grandl, J., Spencer, K. S., Kim, S. E., Schmidt, M., Mathur, J., Dubin, A. E., Montal, M., and Patapoutian, A. (2012) Piezo proteins are pore-forming subunits of mechanically activated channels. *Nature* **483,** 176–181
43. Gevaert, T., Vriens, J., Segal, A., Everaerts, W., Roskams, T., Talavera, K., Owsianik, G., Liedtke, W., Daelemans, D., Dewachter, I., Van Leuven, F., Voets, T., De Ridder, D., and Nilius, B. (2007) Deletion of the transient receptor potential cation channel TRPV4 impairs murine bladder voiding. *J. Clin. Invest.* **117,** 3453–3462
44. Wang, E. C., Lee, J. M., Ruiz, W. G., Balestreire, E. M., von Bodungen, M., Barrick, S., Cockayne, D. A., Birder, L. A., and Apodaca, G. (2005) ATP and purinergic receptor-dependent membrane traffic in bladder umbrella cells. *J. Clin. Invest.* **115,** 2412–2422
45. Jin, M., Wu, Z., Chen, L., Jaimes, J., Collins, D., Walters, E. T., and O'Neil, R. G. (2011) Determinants of TRPV4 activity following selective activation by small molecule agonist GSK1016790A. *PLoS One* **6,** e16713
46. McHugh, B. J., Buttery, R., Lad, Y., Banks, S., Haslett, C., and Sethi, T. (2010) Integrin activation by Fam38A uses a novel mechanism of R-Ras targeting to the endoplasmic reticulum. *J. Cell Sci.* **123,** 51–61
47. Becker, D., Bereiter-Hahn, J., and Jendrach, M. (2009) Functional interaction of the cation channel transient receptor potential vanilloid 4 (TRPV4) and actin in volume regulation. *Eur. J. Cell Biol.* **88,** 141–152
48. Janssen, D. A., Hoenderop, J. G., Jansen, K. C., Kemp, A. W., Heesakkers, J. P., and Schalken, J. A. (2011) The mechanoreceptor TRPV4 is localized in adherence junctions of the human bladder urothelium: a morphological study. *J. Urol.* **186,** 1121–1127
49. Dunning-Davies, B. M., Fry, C. H., Mansour, D., and Ferguson, D. R. (2013) The regulation of ATP release from the urothelium by adenosine and transepithelial potential. *BJU Int.* **111,** 505–513
50. Darby, M., Kuzmiski, J. B., Panenka, W., Feighan, D., and MacVicar, B. A. (2003) ATP released from astrocytes during swelling activates chloride channels. *J. Neurophysiol.* **89,** 1870–1877
51. Anderson, C. M., Bergher, J. P., and Swanson, R. A. (2004) ATP-induced ATP release from astrocytes. *J. Neurochem.* **88,** 246–256
52. Miyaji, T., Sawada, K., Omote, H., and Moriyama, Y. (2011) Divalent cation transport by vesicular nucleotide transporter. *J. Biol. Chem.* **286,** 42881–42887
53. Sawada, K., Echigo, N., Juge, N., Miyaji, T., Otsuka, M., Omote, H., Yamamoto, A., and Moriyama, Y. (2008) Identification of a vesicular nucleotide transporter. *Proc. Natl. Acad. Sci. U.S.A.* **105,** 5683–5686
54. Stout, C. E., Costantin, J. L., Naus, C. C., and Charles, A. C. (2002) Intercellular calcium signaling in astrocytes via ATP release through connexin hemichannels. *J. Biol. Chem.* **277,** 10482–10488
55. Sorensen, C. E., and Novak, I. (2001) Visualization of ATP release in pancreatic acini in response to cholinergic stimulus. Use of fluorescent probes and confocal microscopy. *J. Biol. Chem.* **276,** 32925–32932
56. Maroto, R., and Hamill, O. P. (2001) Brefeldin A block of integrin-dependent mechanosensitive ATP release from Xenopus oocytes reveals a novel mechanism of mechanotransduction. *J. Biol. Chem.* **276,** 23867–23872
57. Bodin, P., and Burnstock, G. (2001) Evidence that release of adenosine triphosphate from endothelial cells during increased shear stress is vesicular. *J. Cardiovasc. Pharmacol.* **38,** 900–908
58. Chai, T. C., and Keay, S. (2004) New theories in interstitial cystitis. *Nat. Clin. Pract. Urol.* **1,** 85–89
59. Graham, E., and Chai, T. C. (2006) Dysfunction of bladder urothelium and bladder urothelial cells in interstitial cystitis. *Curr. Urol. Rep.* **7,** 440–446
60. Sugaya, K., Nishijima, S., Kadekawa, K., Miyazato, M., and Mukouyama, H. (2009) Relationship between lower urinary tract symptoms and urinary ATP in patients with benign prostatic hyperplasia or overactive bladder. *Biomed. Res.* **30,** 287–294